JOURNAL OF AIRCRAFT
Vol. 48, No. 1, January–February 2011

Framework for Establishing Limits of Tabular Aerodynamic Models for Flight Dynamics Analysis

M. Ghoreyshi,* K. J. Badcock,† A. Da Ronch,‡ S. Marques,‡ A. Swift,§ and N. Ames¶
University of Liverpool, Liverpool, UK, L69 3GH

DOI: 10.2514/1.C001003

This paper describes the use of the Euler equations for the generation and testing of tabular aerodynamic models for flight dynamics analysis. Maneuvers for the AGARD Standard Dynamics Model sharp leading-edge wind-tunnel geometry are considered as a test case. Wind-tunnel data is first used to validate the prediction of static and dynamic coefficients at both low and high angles, featuring complex vortical flow, with good agreement obtained at low to moderate angles of attack. Then the generation of aerodynamic tables is described based on a data fusion approach. Time-optimal maneuvers are generated based on these tables, including level flight trim, pull-ups at constant and varying incidence, and level and 90 ° turns. The maneuver definition includes the aircraft states and also the control deflections to achieve the motion. The main point of the paper is then to assess the validity of the aerodynamic tables which were used to define the maneuvers. This is done by replaying them, including the control surface motions, through the time accurate computational fluid dynamics code. The resulting forces and moments are compared with the tabular values to assess the presence of inadequately modeled dynamic or unsteady effects. The agreement between the tables and the replay is demonstrated for slow maneuvers. Increasing rate maneuvers show discrepancies which are ascribed to vortical flow hysteresis at the higher rate motions. The framework is suitable for application to more complex viscous flow models, and is powerful for the assessment of the validity of aerodynamics models of the type currently used for studies of flight dynamics.

Nomenclature

b	=	wing span, m
C_D	=	drag coefficient
C_L	=	lift coefficient
$C_{L_{\dot{\alpha}}}$	=	derivative of lift coefficient with angle of attack rate
$\bar{C}_{L\alpha}$, $\bar{C}_{Lq}$	=	in and out phase components of lift coefficients
$C_{L\alpha}$	=	lift slope with respect to angle of attack
C_{L_q}	=	derivative of lift coefficient with respect to pitch rate
C_{l_p}	=	derivative of rolling moment coefficient with respect to roll rate
C_{l_r}	=	derivative of rolling moment coefficient with respect to yaw rate
C_m	=	pitching moment coefficient
$C_{m_{\dot{\alpha}}}$	=	derivative of pitching moment coefficient with angle of attack rate
$C_{m\alpha}$	=	pitching moment coefficient slope with respect to angle of attack
C_{m_q}	=	derivative of pitching moment coefficient with respect to pitch rate
C_N, C_Z	=	normal and downward normal force coefficients
C_n	=	yawing moment coefficient
C_{n_r}	=	derivative of yawing moment coefficient with respect to yaw rate
C_{n_p}	=	derivative of yawing moment coefficient with respect to roll rate
C_{roll}	=	rolling moment coefficient
C_Y	=	side-force coefficient
C_{y_p}	=	derivative of side-force coefficient with respect to roll rate
C_{y_r}	=	derivative of side-force coefficient with respect to yaw rate
c	=	wing chord, m
E	=	end point cost function
e	=	event constraints
F	=	running cost function
f	=	residual vector of equations of motion
H	=	Hamiltonian Function
h	=	control/path constraints
I_{ij}	=	moment of inertia components
J	=	cost function for maneuver optimization
k	=	reduced frequency of the periodic motion
m	=	aircraft mass
$\dot{q}$	=	time rate of pitch rate, rad/s^2
q	=	pitch rate, rad/s
S	=	wing area, m^2
T	=	thrust force, N
T_m	=	maximum thrust force, N
t_0	=	initial time, s
t_f	=	final time, s
t	=	time, s
u	=	vector of aircraft controls
V_0	=	initial speed, m/s
v	=	aircraft velocity vector
x	=	vector of aircraft states
α	=	angle of attack
α_A	=	amplitude of forced pitching motion
Δt	=	time step, s
λ	=	costate variable
ω	=	frequency of periodic motion

Presented as Paper 2009 at the AIAA Guidance, Navigation, and Control Conference, Chicago, 10–13 August 2009; received 23 October 2009; revision received 17 September 2010; accepted for publication 21 September 2010.

*Research Assistant, Department of Engineering.
†Professor, SMAIAA, Department of Engineering; K.J.Badcock@liverpool.ac.uk. (Corresponding Author).
‡Research Assistant, Department of Engineering.
§Ph.D. Student, Department of Engineering.
¶Undergraduate Student, Department of Engineering.

I. Introduction

FLIGHT mechanics analysis of combat aircraft requires a nonlinear and unsteady aerodynamic model valid for rapid and large amplitude maneuvers [1,2]. The source of nonlinearity and unsteadiness is mainly due to shock waves, separation, and vortices

[3]. These phenomena impact aircraft performance, but developing a model of the forces and moments for these flows is difficult due to the complexity of flow simulation and the limitations of existing dynamic wind-tunnel test facilities [4]. Current industrial practice is to develop aerodynamic models based on wind-tunnel testing, placing constraints on how much detailed analysis can be carried out early in the development phase of an aircraft. Computational methods do not in principle suffer from this limitation. Prior attempts at exploiting computational fluid dynamics (CFD) for predicting S and C derivatives were reported in [5–9]. The use of CFD as a source of aerodynamic data incurs a significant computational cost if very large numbers of calculations, particularly of the unsteady variety, are required. The cost comes both from the large number of cases potentially required (hundreds to tens of thousands) and the cost of individual simulations (which can require large scale calculations on supercomputers for detached eddy simulation of maneuvering aircraft due to the range of time scales that must be resolved).

The aerodynamic model for flight dynamics analysis considered in this paper is tabular in form. Tables are consistent with quasi-steady aerodynamics for a wide range of flight conditions, but have several associated difficulties. First, a large number of table entries must be filled. The brute-force calculation of the entire table using CFD is not feasible due to computational cost. Sampling and data fusion methods have been proposed to overcome this [10]. Secondly, the precomputed nature of tables lacks the ability to describe hysteresis of the aerodynamic phenomena. That flow hysteresis impacts on the manoeuvering aircraft was first recognized by Harper and Flanigan [11] in 1950. They showed that there is a substantial increase of aircraft lift force if the aircraft is pitched at a rapid rate. It is well known that aerodynamic forces and moments of aircraft responding to sudden rate changes not only depend on the instantaneous states but also their time histories [12–14]. Abramov et al. [15] mention that the normalized time-lags in aerodynamic loads from vortex breakdown phenomena can be up to 15 times bigger than the convective time scale.

CFD tools are becoming credible for the computation of aerodynamic time history effects. The flight dynamics of a manoeuvering aircraft could potentially be modeled by coupling the unsteady Reynolds-averaged Navier–Stokes (URANS) equations and the dynamic equations governing the aircraft motion. First attempts were limited to two-dimensional test cases [16–19], while recently the coupled CFD-flight dynamics of a full aircraft has been studied [20]. However, the CFD-flight dynamics simulations take substantially longer than when taking the forces and moments from look-up tables raising the open question of when time history of the aerodynamics is required for flight dynamics analysis.

In the present paper a framework for investigating the limits, from flow unsteadiness, of aerodynamic tables is described. The particular demonstrations of this framework are made for a generic (and sharp leading-edge) fighter performing time-optimal maneuvers with the aerodynamics given by the Euler equations. The paper first summarises the flow solver and how the maneuvers are computed. Then the test case is described and the aerodynamic predictions validated. The generation of the aerodynamic tables and the approach to defining the time-optimal maneuvers is then given. The evaluation of the aerodynamic tables for these maneuvers is then made by replaying them directly through an unsteady CFD calculation. Finally, conclusions are given.

II. CFD Formulation

A. Flow Code

The flow solver used for this study is the University of Liverpool Parallel Multi-Block solver. The Euler and RANS equations are discretized on curvilinear multiblock body conforming grids using a cell-centered finite volume method which converts the partial differential equations into a set of ordinary differential equations. The equations are solved on block structured grids using an implicit solver which uses Krylov subspace solutions arising from an approximate linearization of the CFD residual [21], Osher and Chakravarthy's method for the discretisation of the fluxes [22] and monotone upwind scheme for conservation laws interpolsation [23] for second-order accuracy. A wide variety of unsteady flow problems, including aeroelasticity, cavity flows, aerospike flows, delta wing aerodynamics, rotorcraft problems, and transonic buffet have been studied using this code. More details on the flow solver can be found in Badcock et al. [21] and a validation against flight data for the F-16XL aircraft is made in [24].

B. Motion Replay

The key functionality for the CFD solver in the current application is the ability to move the mesh. Two types of mesh movement are required. First, a rigid rotation and translation is needed to follow the motion of the aircraft. Secondly, the control surfaces are deflecting throughout the motion. The control surfaces are blended into the geometry following the approach given in [25]. After the surface grid point deflections are specified, transfinite interpolation is used to distribute these deflections to the volume grid.

The rigid motion and the control deflections are both specified from a motion input file. For the rigid motion the location of a reference point on the aircraft is specified at each time step. In addition the rotation of the aircraft about this reference point is also defined. Mode shapes are defined for the control surface deflections [26]. Each mode shape specifies the displacement of the grid points on the aircraft surface for a particular control surface. These are prepared as a preprocessing step using a utility that identifies the points on a control surface, defines the hinge, rotates the points about the hinge, and works out their displacements. The motion input file

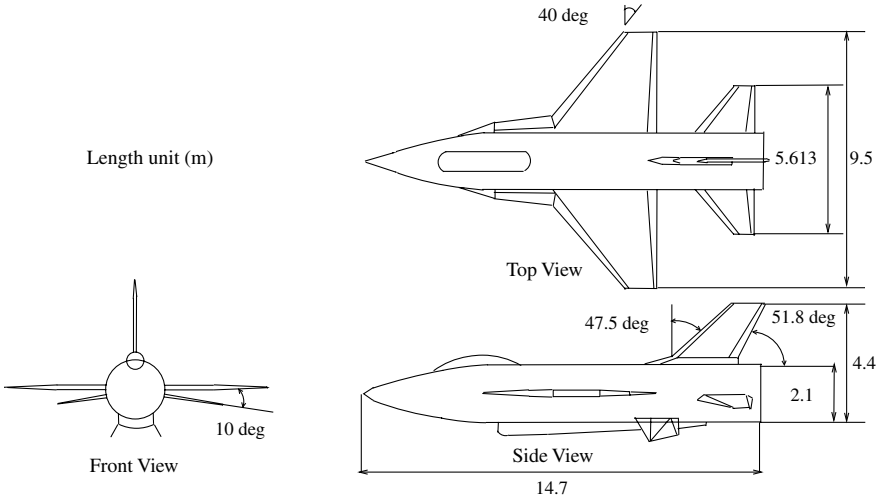

Fig. 1 SDM layout adapted from [33].

then defines a scaling factor for each mode shape to achieve the desired control surface rotation.

The desired motion to be replayed through the unsteady CFD solution is specified in the motion input file. The aircraft reference point location, rotation angles, and control surface scaling factors are needed. The rotation angles are given by the pitch, yaw, and bank angles. The aircraft reference point velocity $\mathbf{v}_a$ in an inertial frame is then calculated to achieve the required angles of attack and side slip, and the forward speed. The velocity is then used to calculate the location. The CFD solver was originally written for steady external aerodynamics applications. The wind direction and Mach number are specified for a steady case. If the initial aircraft velocity is denoted as $\mathbf{v}_0$, then this vector is used to define the Mach number and the angle of attack for the steady input file (specifying the fixed freestream wind velocity used throughout the calculation). Then the instantaneous aircraft location for the motion file is defined from the relative velocity vector $\mathbf{v}_a - \mathbf{v}_0$.

III. Test Case and Validation

The Standard Dynamics Model (SDM) is a generic fighter configuration based on the F-16 planform. The model includes a slender strake-delta wing, horizontal and vertical stabilizers, ventral fin and a blocked off inlet. The three view drawing is shown in Fig. 1. This geometry has been used to collect wind-tunnel data [27–30].

In the current paper the Euler calculations are used to generate the aerodynamic forces and moments. A block structured mesh was generated. The geometry was slightly simplified by removing the blocked off intake and the ventral fins. Because the main interest here is on the impact of vortical flow on the upper lifting surfaces these were considered reasonable simplifications. A fine Euler mesh was generated with 5.6 million points, and a coarse mesh was obtained with 701 thousand points by omitting every second point in each dimension. The calculations described are for the coarse mesh unless otherwise stated.

Mesh block faces were placed on the control surfaces and the mesh points on these faces were deflected to define the control surface mode shapes. The control surfaces are blended into the airframe as described above, and views of the surface mesh for the deflected control surfaces are shown in Fig. 2.

The geometric, mass, inertial, and engine properties of the SDM are obtained from data in Winchenbach et al. [31]. Their free-flight model is 0.1325:1 scale of the studied model in this paper resulting in scaled-up values of:

$$S = 27.87\ \text{m}^2 \qquad m = 9295.44\ \text{kg} \qquad c = 3.45\ \text{m}$$

$$I_{xx} = 12874.0\ \text{kg m}^2 \qquad b = 9.144\ \text{m} \qquad I_{yy} = 75673.0\ \text{kg m}^2$$

$$T_m = 26.24\text{KN} I_{zz} = 85552.0\text{kgm}^2$$

where T_m is the maximum total thrust force assumed to cross the center of gravity. The direction of the thrust relative to the aircraft is assumed to remain unchanged with altitude and flight speed, and to vary linearly with the engine throttle.

The lifting surfaces all have sharp leading edges. This allows the Euler equations to approximate the development of vortical flow because the separation points are fixed at the leading edge. A complex interaction of the strake and wing vortices develops as the incidence is increased, as illustrated in Fig. 3 for low-speed and no side-slip conditions. At ten degrees the vortices form, do not exhibit breakdown and do not interact over the airframe. At 15 degrees the two vortices wind around each other toward the trailing edge of the wing. At 20 degrees the wing vortex appears to breakdown quickly after formation, whereas the strake vortex is coherent for longer. Finally, at 30 degrees there is no sign of coherent vortices. Note that these calculations were all run as steady state although vortical interactions and the separated flowfield do have high-frequency aerodynamic variations. The assumption is that the high-frequency variations from the natural unsteadiness of the flow are at a much lower amplitude than the variations due to the aircraft maneuvers, and can therefore be neglected. This was tested by running time

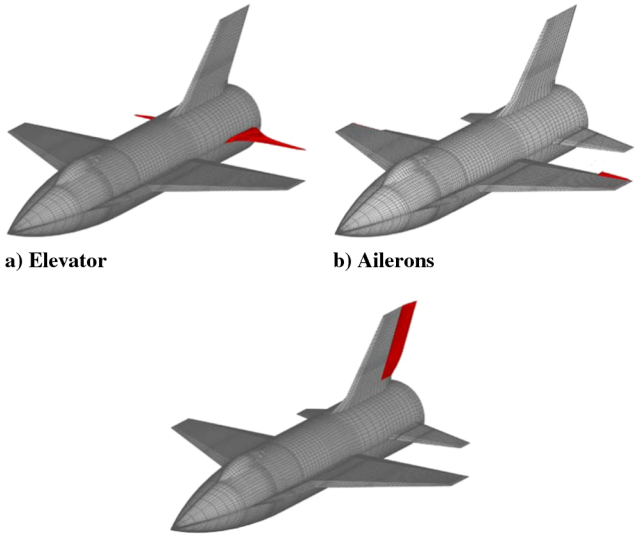

Fig. 2 View of deflected control surfaces on the surface grid.

accurate calculations with small time steps for a fixed angle of attack of 15 deg and a Mach number of 0.3, and comparing the time histories of the forces and moments with the predictions from a steady-state calculation. The unsteady calculations used 10,000 and 50,000 real time steps for a nondimensional time duration of 50 (nondimensionalized with respect to the freestream velocity and root chord) which corresponds to about 1.7 s. This comparison for the normal force is shown in Fig. 4. The coarse grid unsteady calculation reaches a steady state. In contrast the fine grid shows a small oscillation around the steady-state value. The solutions using 10,000 and 50,000 time steps are virtually identical. Note that the fluctuations seen in the figure are small compared with those arising from the flight maneuvers that are the focus of this paper. It is therefore felt justified to neglect this component of the unsteadiness for the remainder of this paper.

These vortex dominated flowfields cause nonlinear variations in the aerodynamic forces and moments. Figure 5 compares DATCOM [32] and CFD results with available experimental data [33] at low-speed and zero side-slip conditions. The pitching moment for these comparisons is taken about the aircraft node. The figures show that there is a good agreement between the Euler predictions and the measurements for angles of attack below 20 deg. Above 20 deg the disagreement in the magnitude of the longitudinal quantities increases and the sign of the slope of the lateral quantities is wrong. At these conditions it was seen that the coherent vortical flow is lost, and the lateral forces and moments will be strongly influenced by the separated flow adjacent to the vertical fin. In addition the ventral fins were omitted in the computations and this may contribute to the discrepancies. The Euler simulations do not predict this flowfield properly, and detached eddy simulation would be a better option. The DATCOM predictions in some respects are adequate (e.g., for the pitching moment and normal force coefficient), but it should be noted that the empirical database which underlies these predictions is for a conventional aircraft which would not feature vortical flow. This can be seen in the predictions of the normal force coefficient which show a conventional aircraft stall. The lateral coefficients are generally not well predicted by DATCOM in this case. Also shown are the Euler predictions on the fine grid and these are in close agreement to the coarse results.

For fast maneuvers the dynamic contributions to the forces and moments are required. The estimation of the quasi-steady dynamic derivatives is achieved by imposing a forced sinusoidal motion around the aircraft center of gravity. For the extraction of longitudinal dynamic derivative values from time-histories of the forces and moments, it is assumed that the aerodynamic coefficients are linear functions of the angle of attack α, pitching angular velocity q, and rate, $\dot{q}$. To illustrate, the increment in the lift coefficient with respect

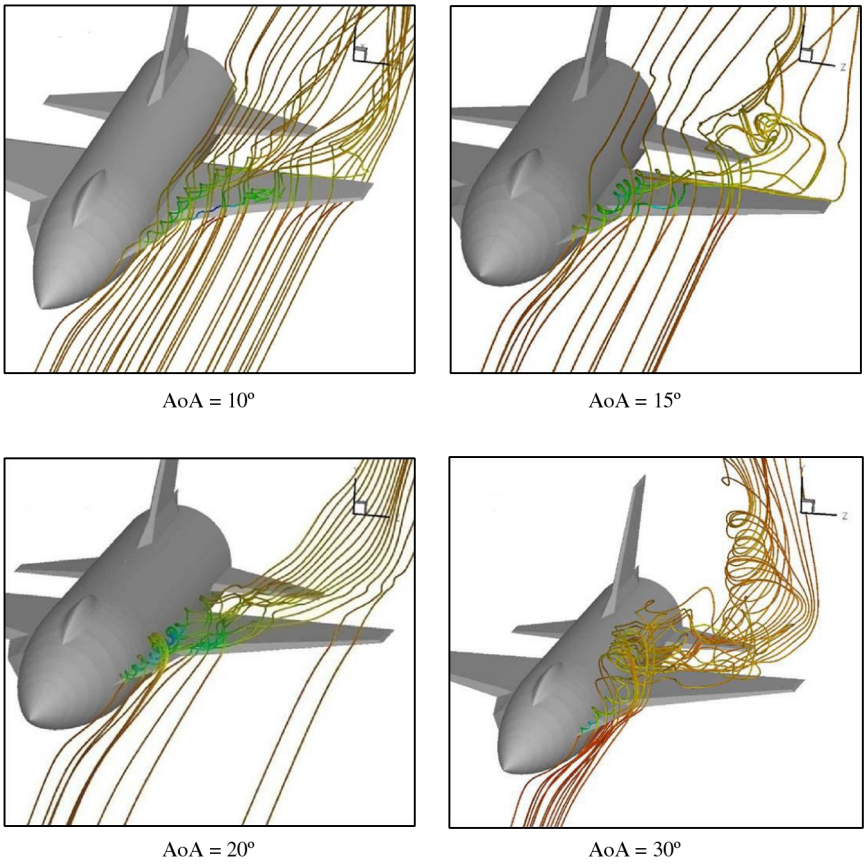

Fig. 3 SDM flowfield visualization using streamlines shaded by pressure coefficient. The calculations are for a Mach number of 0.3 and 0 deg side slip.

to its mean value during the applied sinuisoidal motion is formulated as

$$\Delta C_L = C_{L_\alpha}\Delta\alpha + \frac{c}{V}C_{L_{\dot\alpha}}\dot\alpha + \frac{c}{V}C_{L_q}q + \left(\frac{c}{V}\right)^2 C_{L_{\dot q}}\dot q \qquad (1)$$

where V is the magnitude of the aircraft velocity vector and c is the wing root chord.

The harmonic motion defines the relations

$$\Delta\alpha = \alpha_A \sin(\omega t) \qquad \dot\alpha = \alpha_A \omega \cos(\omega t) \qquad \dot q = -\alpha_A \omega^2 \sin(\omega t) \qquad (2)$$

Equation (1) can be rewritten as

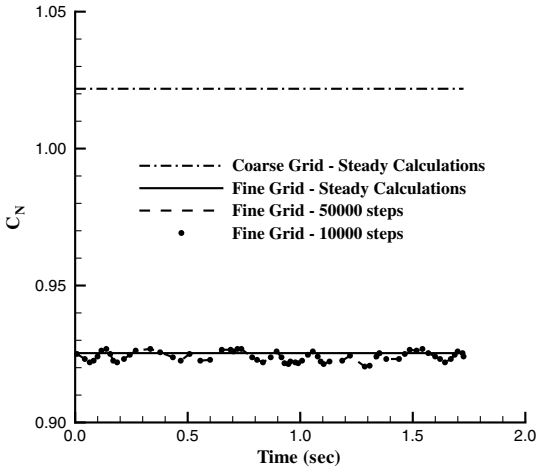

Fig. 4 SDM fixed geometry unsteady calculations for a Mach number of 0.3, zero side slip, and an angle of attack of 15 deg.

$$\Delta C_L = \alpha_A(C_{L_\alpha} - k^2 C_{L_{\dot q}})\sin(\omega t) + \alpha_A k(C_{L_{\dot\alpha}} + C_{L_q})\cos(\omega t) \qquad (3)$$

where $k = c\omega/V$ is the reduced frequency of the applied motion. The in-phase and out-of-phase components of ΔC_L, respectively, indicated as $\bar C_{L_\alpha}$ and $\bar C_{L_q}$, can be defined as

$$\bar C_{L_\alpha} = C_{L_\alpha} - k^2 C_{L_{\dot q}} \qquad (4)$$

$$\bar C_{L_q} = C_{L_{\dot\alpha}} + C_{L_q} \qquad (5)$$

and then

$$\Delta C_L = \alpha_A \bar C_{L_\alpha}\sin(\omega t) + \alpha_A k \bar C_{L_q}\cos(\omega t) \qquad (6)$$

These coefficients can be obtained by taking the first Fourier coefficients of the time history of C_L.

The longitudinal dynamic derivatives were computed for the SDM. Periodic motions with five degrees amplitude and a reduced frequency of 0.0493 were applied for six cycles to reach a periodic state. Figure 6 shows the comparison with wind-tunnel data from references [29,30]. A good quantitative agreement is obtained on the coarse grid. Note that the pitching moment values in the comparison are taken about a location 53% along the fuselage. The solutions using 40 and 80 steps per cycle yield very similar results. The magnitude of the peaks in the normal and moment coefficients are mesh dependent, which is not unexpected for Euler solutions which rely on numerical diffusion in the region of the leading edge for the generation of vorticity. While this limitation could be improved by using viscous modeling, it is considered that the Euler solutions for this case are adequate to allow the development of the framework for the generation of tables and the replay of maneuvers for a test case which has qualitatively correct flow behavior.

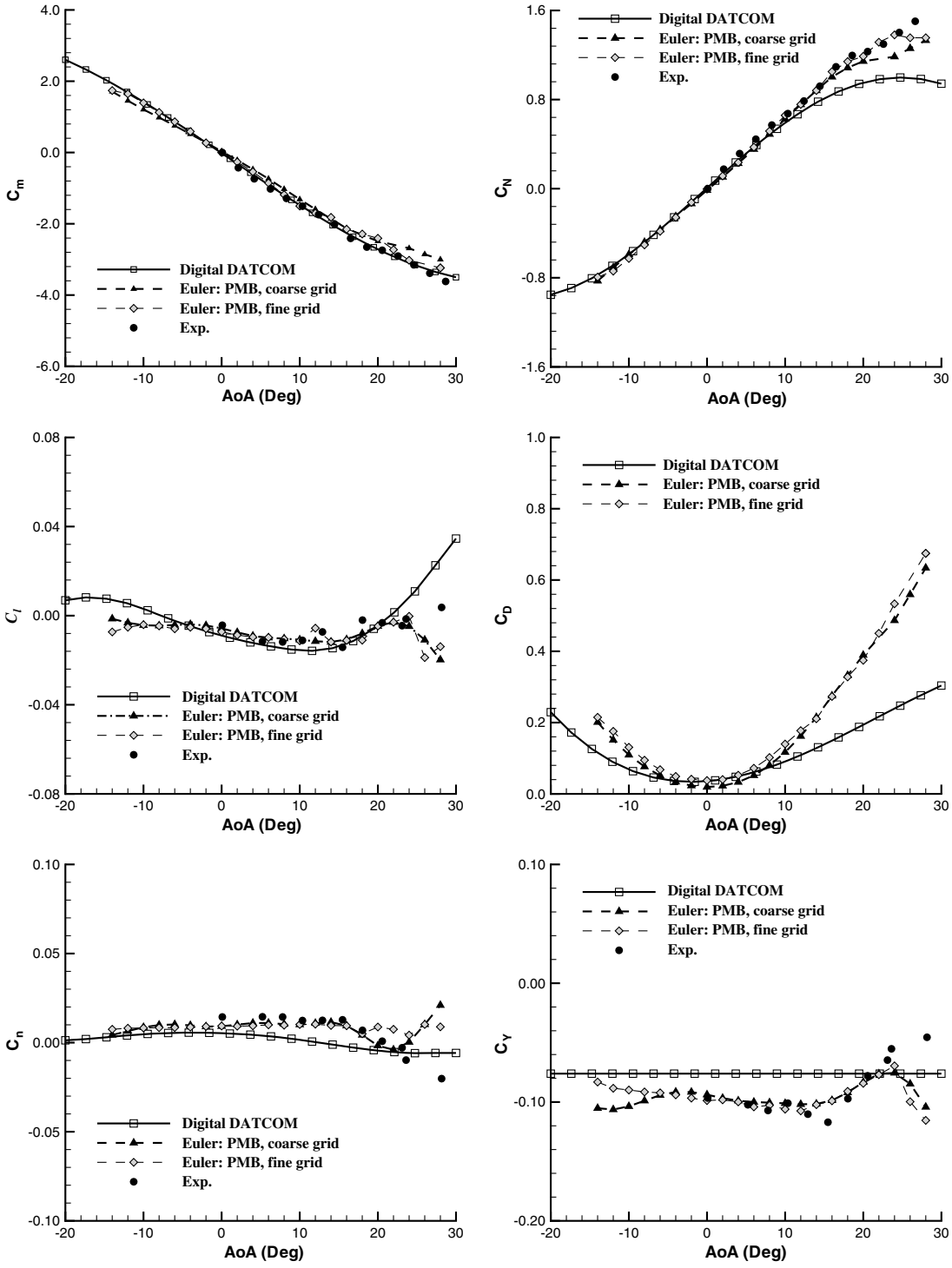

Fig. 5 Static aerodynamic predictions: lift, drag, and pitching moments are for 0 deg side slip and a Mach number of 0.3. The lateral figures are for 5 deg of side slip and a Mach number of 0.3. The experimental data are from [33].

IV. Generation of Maneuvers

A. Aerodynamic Tables

Flight dynamics predictions require a vector of aerodynamic forces and moments

$$[C_L, C_D, C_m, C_Y, C_l, C_n]^T$$

representing wind axis coefficients of lift, drag, pitching moment, side-force, rolling moment, and yawing moment coefficient, respectively. This vector depends on the aircraft state and control variables. In this paper, this dependency is represented in look-up tables. For a slow motion, the aerodynamic forces and moments are assumed to depend on angle of attack, Mach number, side-slip angle, and three control surface deflection angles. The tables are arranged with three parameters in each: Mach number, angle of attack and one other variable. Around 6000 entries are required to define the variations in each table, leading to a large number of calculations required if a brute force method was used.

An alternative approach is used to fill up the tables. The brute-force calculations were used to provide the values with respect to the angle of attack and Mach number (referred to here as the baseline table). The dependence of the longitudinal forces and moments on other parameters is assumed to be an increment of the baseline table and the Co-Kriging data fusion method [10] is used to include this variation

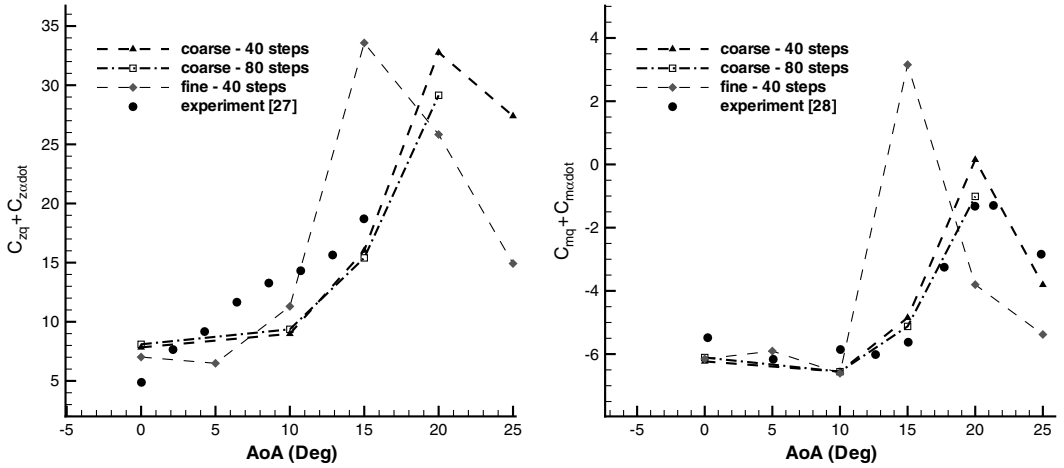

Fig. 6 Out-of-phase dynamic derivative aerodynamic predictions. The Mach number is 0.3 and the mean side-slip angle is zero.

in a computationally efficient way. Kriging defines values reconstructured from available samples by estimating correlations between the known and unknown values. Co-Kriging exploits the correlation established for one set of data (in this case for the Mach number and angle of attack variation) to build the correlation for a related data set. The baseline table describes the general trends of longitudinal aerodynamic forces and moments. This table consists of 156 conditions, with the angle of attack ranging from −14 to 28°, and the Mach number from 0.1 to 0.4. With just 15 additional samples the variation with the elevator, side-slip angle, aileron, and rudder was included in the tables. The replay solutions described below provide a test of these tables.

For the lateral coefficients a different approach is needed because all the lateral coefficients in the baseline table are zero. Instead the DATCOM lateral coefficients are used as low fidelity data to initialize the tables, and then Co-Kriging with a few Euler results are used to generate updated tables.

For the dynamic derivatives, these are assumed to be independent of Mach number, and to vary only with angle of attack. This follows the suggestion from the experimental study described in [31].

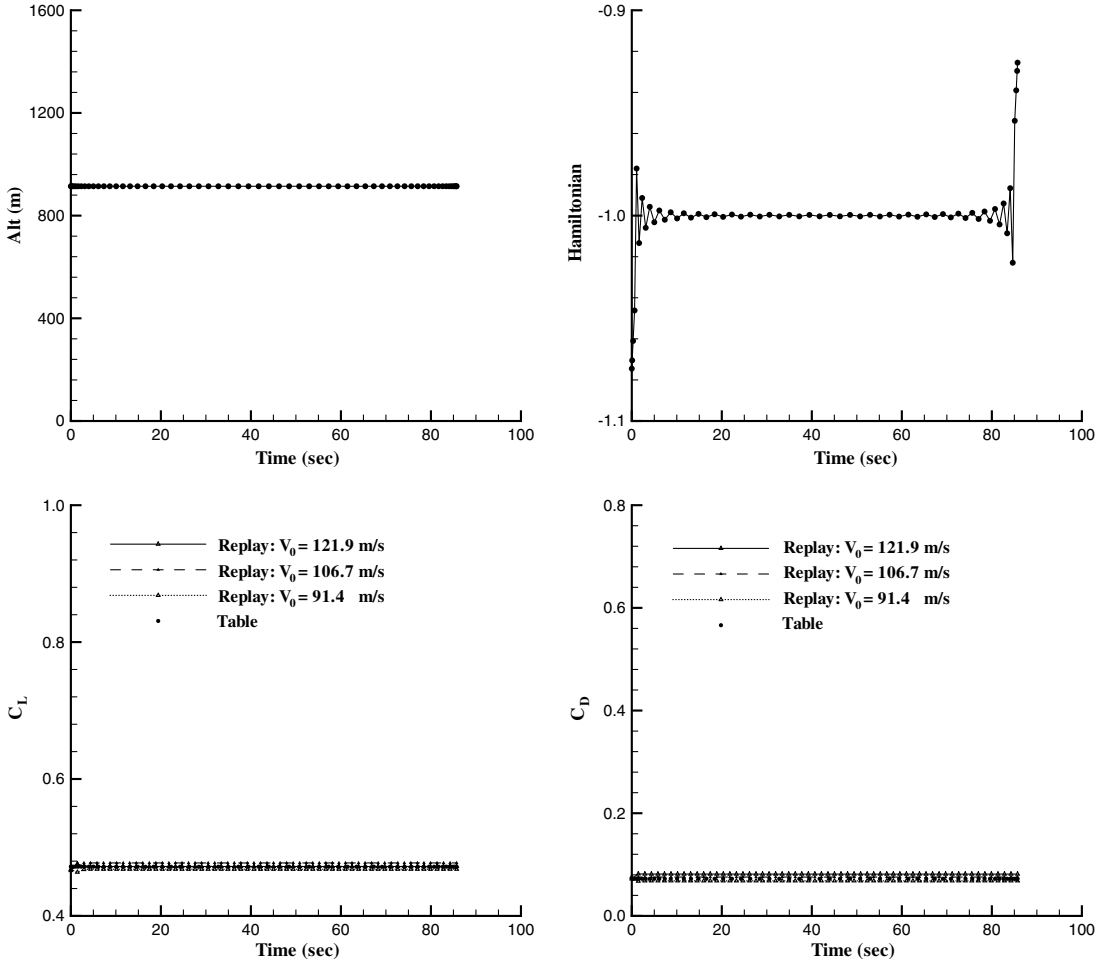

Fig. 7 Level flight trim solution and replay test.

B. Time-Optimal Maneuvers

This paper aims to investigate the validity of the aerodynamic tables for the generation of time-optimal maneuvers. Maneuver flight [34] is the response of the aircraft to the pilot's applied control inputs starting from one trimmed flight condition to another. The maneuver time is the period between the initial and final trim points, and this should be minimized for aerial combat maneuvers.

The optimal control problem finds the optimal controls that move the aircraft from the initial state to the final state while minimizing a specified cost function [35]. The optimal control aims to find a state-control pair (x, u) and the final time t_f that minimizes the cost function

$$J[x(\,), u(\,), t_0, t_f] = E(x(t_0), u(t_f), t_0, t_f) + \int_{t_0}^{t_f} F(x(t), u(t), t)\,\mathrm{d}t \tag{7}$$

where E and F are the endpoint cost and the running cost, respectively. The minimization is subject to the equations of motion, as detailed by Stevens and Lewis [36]. For ease of integration with the look-up tables, the force equations are written in the wind axis

$$\dot{x}(t) = f(x(t), u(t), t) \tag{8}$$

the event constraints

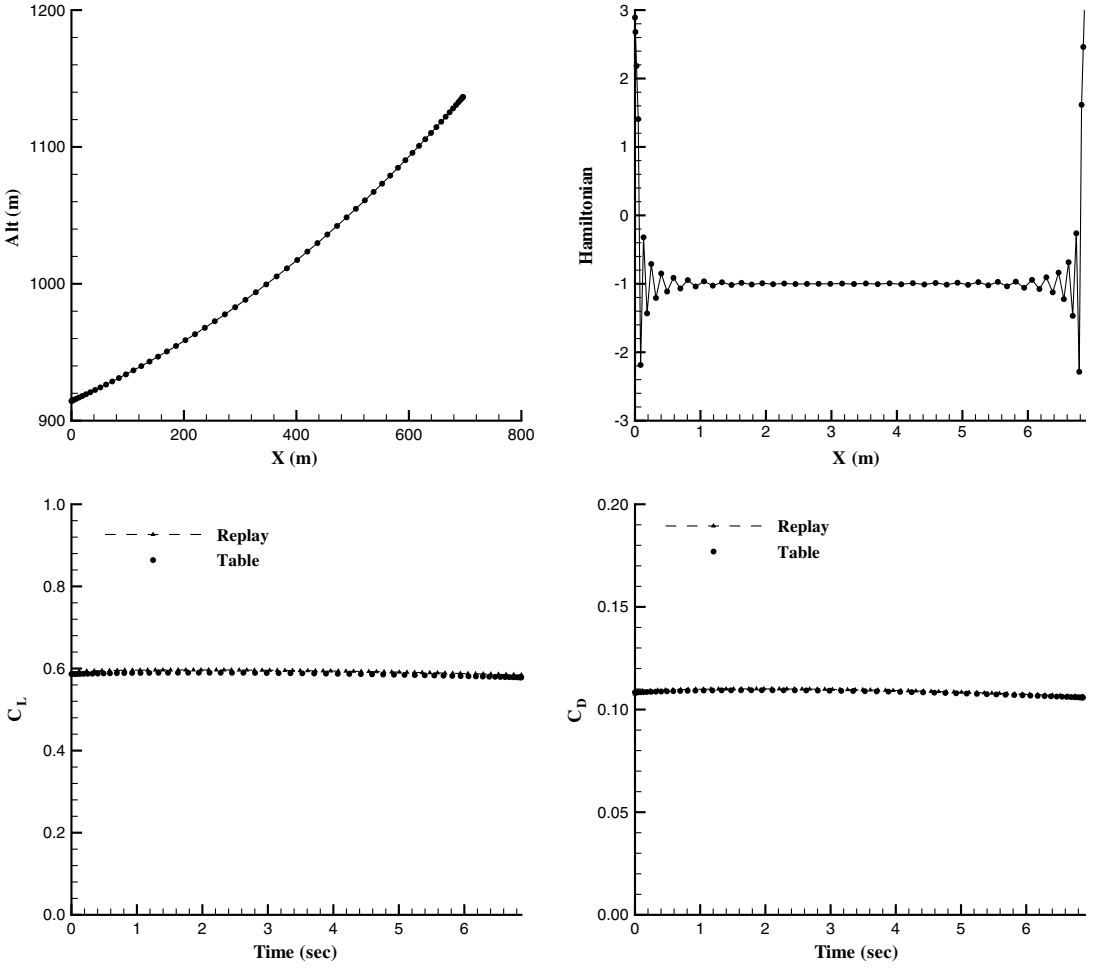

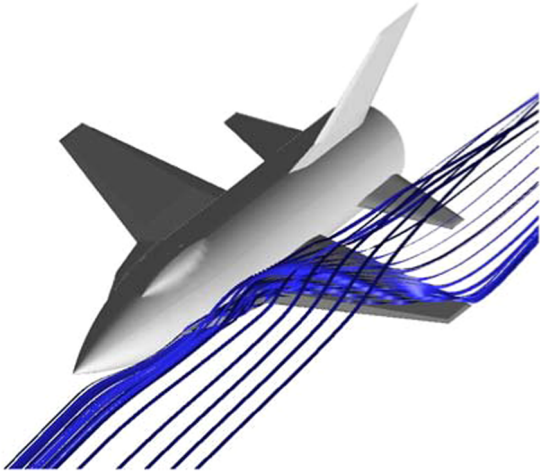

Fig. 8 Steady pull-up maneuver at 2 deg /s pitch rate and a fixed angle of attack of 9.5°.

$$e^L \le e(x(t_0), x(t_f), t_0, t_f) \le e^U \tag{9}$$

the state-control path constraints

$$h^L \le h(x(t), u(t), t) \le h^U \tag{10}$$

and box constraints on the states, controls and clock time

$$\begin{aligned} x^L \le x(t) \le x^U \qquad u^L \le u(t) \le u^U \\ t_0^L \le t_0 \le t_0^U \qquad t_f^L \le t_f \le t_f^U \end{aligned} \tag{11}$$

where L and U denote the lower and upper bound, respectively. A Hamiltonian function is defined by

$$H = F(x(t), u(t), t) + \lambda(t) f(x(t), u(t), t) \tag{12}$$

where $\lambda(t)$ is the costate variable and represents the increment to F resulting from a marginal increase in state parameters. The necessary conditions for optimality are

$$\frac{\partial H}{\partial u} = 0, \qquad \frac{\partial H}{\partial x} = -\dot{\lambda}, \qquad t_0 \le t \le t_f$$

The general aircraft equations of motion detailed in Stevens and Lewis [36] serve as one of the constraints. Also, the initial and final state parameters are fixed with trimmed flight conditions, but the rest of the maneuver is out of trim conditions.

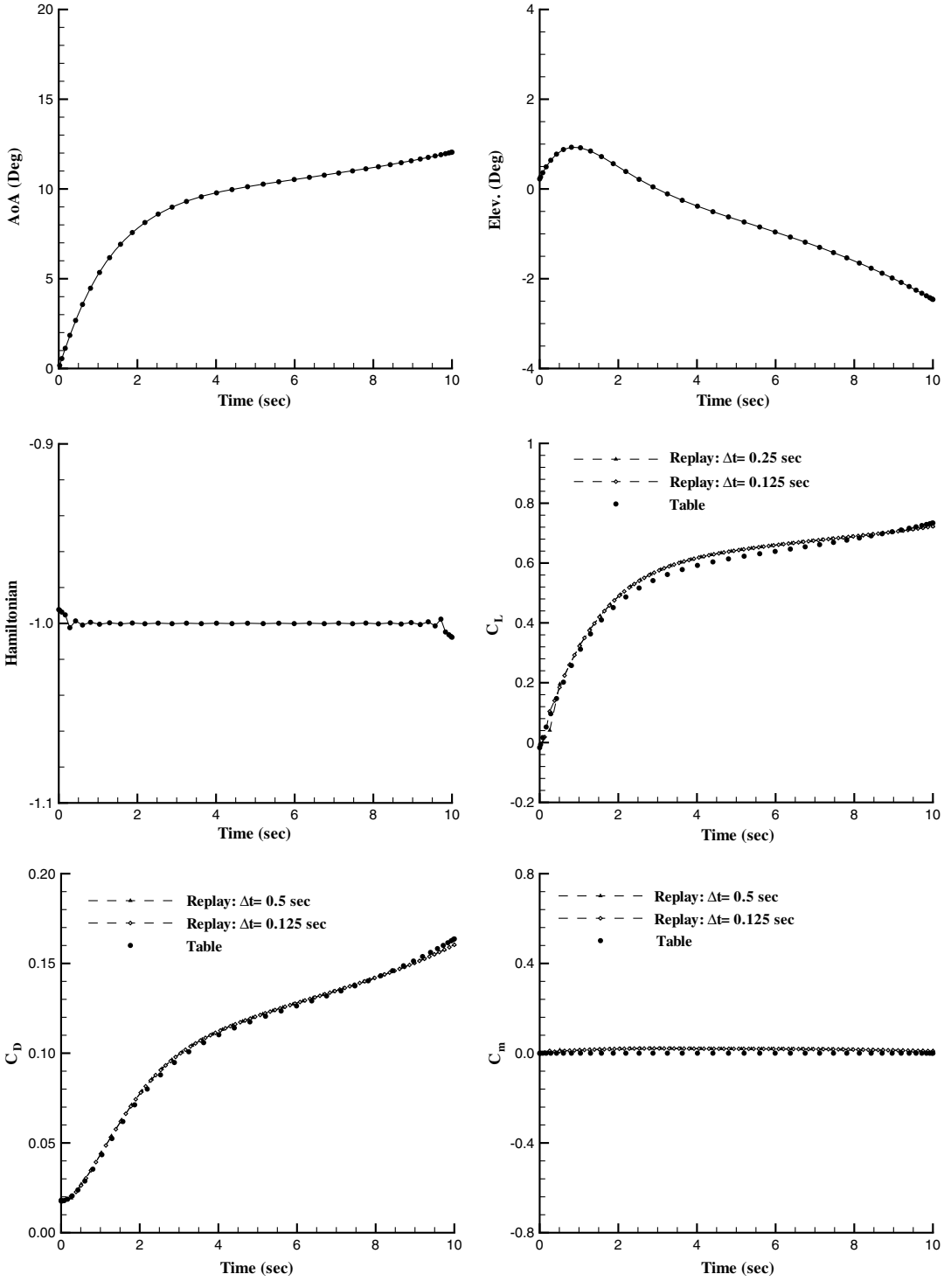

Fig. 9 Slow pull-up maneuver with varying angle of attack.

For the solution of the optimal control problem the DIDO code [37] is used. In DIDO, the time interval is divided into N segments. The boundaries of each time segment are called nodes. The value of N is normally in the range 5 to 150. The optimal state and control pair are calculated at the nodes.

The optimization uses the solution of the equations of motion as a constraint. This solution obtains the aerodynamic forces and moments from the look-up tables. Hence, the predictions from these tables need to be realistic for the maneuver itself to be valid. The validity of the tables can be limited from a number of sources: 1) too coarse a representation, which misses nonlinear variations; 2) inadequate representation of the dynamic derivatives (e.g., neglecting frequency dependence); 3 significant hysteresis in the aerodynamics.

The main contribution of this paper is to consider how to evaluate these limitations by replaying the motion through a time accurate CFD simulation. The predicted forces and moments can then be compared with the tabular model values to evaluate the consistency between the two sets of values.

V. Testing of Maneuver Replay

A. Overview

This section shows the comparison between the prediction of the aerodynamic forces from the static tabular model and the motion replay. This is done for slow motions where close agreement would be expected. The motions used are trimmed level flight, pull-ups with constant and varying angle of attack, wingover and 90-deg turns. The

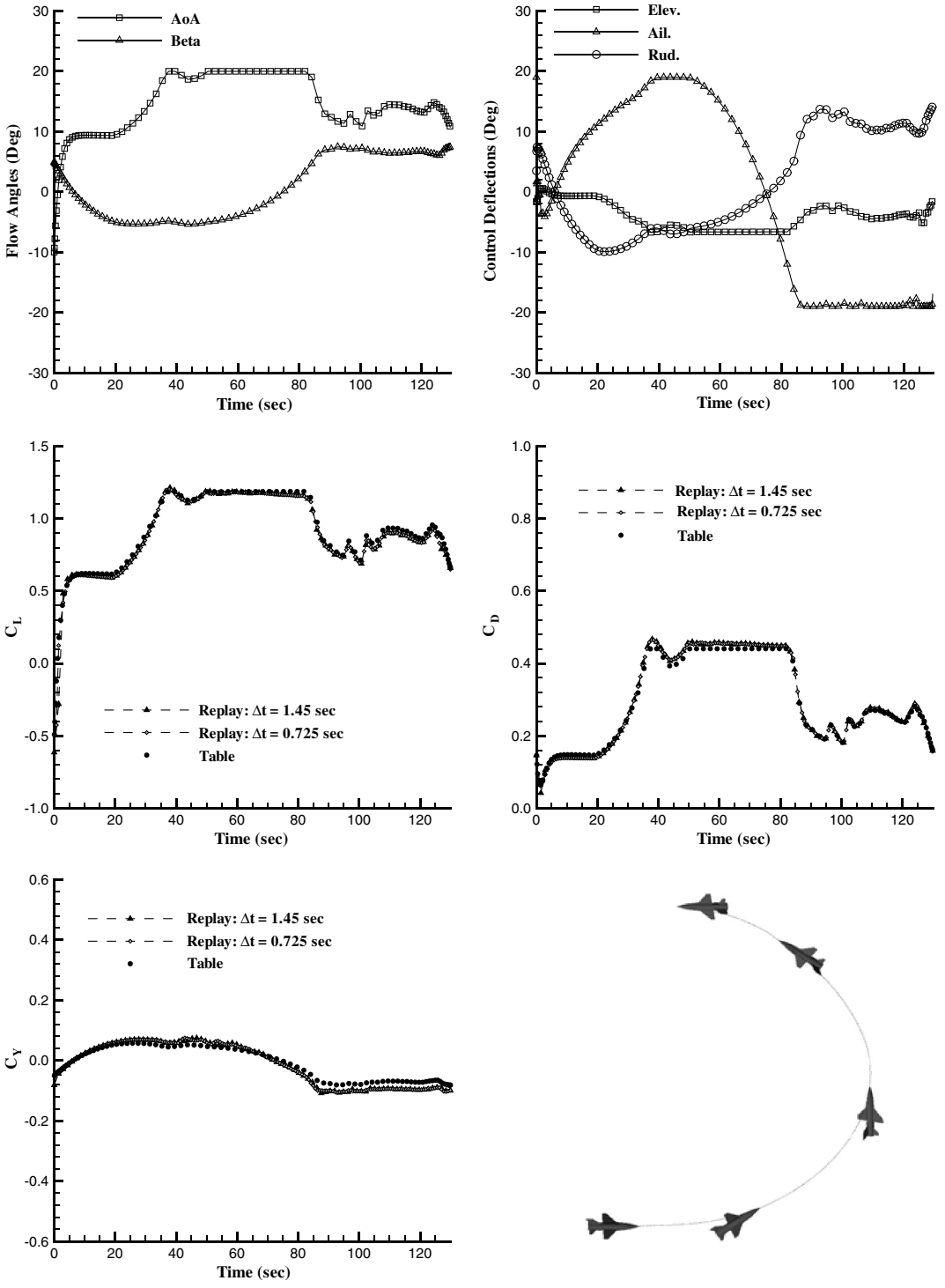

Fig. 10 Wing-over maneuver definition and replay solution.

comparisons test the CFD formulation of the maneuver replay, which is done in a time accurate fashion with control surface deflections. Throughout this section the replay predictions are referred to on the figures as *Replay* and the tabular predictions as *Table*.

B. Trimmed Level Flight

The first maneuver is for steady wing-level straight flight at 914.4 m and 106.7 m/s. To define this maneuver the path constraints are set for the time rates of angle of attack, pitch angle, and flight speed with upper and lower values of $\pm 1.0 \times 10^{-5}$. The solution gives a trim angle of attack 7.67°, elevator deflection angle of 1.69° and 14.7 kN required thrust. To verify the optimal criteria and validate the solution, the Hamiltonian function and flight altitude during flight are shown in Fig. 7. During the 85 s of flight computed the altitude remains unchanged as required. In addition the Hamiltonian values are nearly constant, showing that the solution is optimum.

It is possible to define the replay calculation in different ways. As described in the CFD formulation section the important quantity to be specified is $\mathbf{v}_a - \mathbf{v}_0$ where $\mathbf{v}_0$ is a fixed vector specified through the initial steady-state conditions given to the CFD solver and $\mathbf{v}_a$ is the instantaneous velocity vector of the aircraft in an axis system moving with the initial steady velocity. We are free to choose any steady velocity vector. To test the replay calculation the magnitude of this vector was set to three different values, namely $V_0 = 91.4$, $V_0 =$

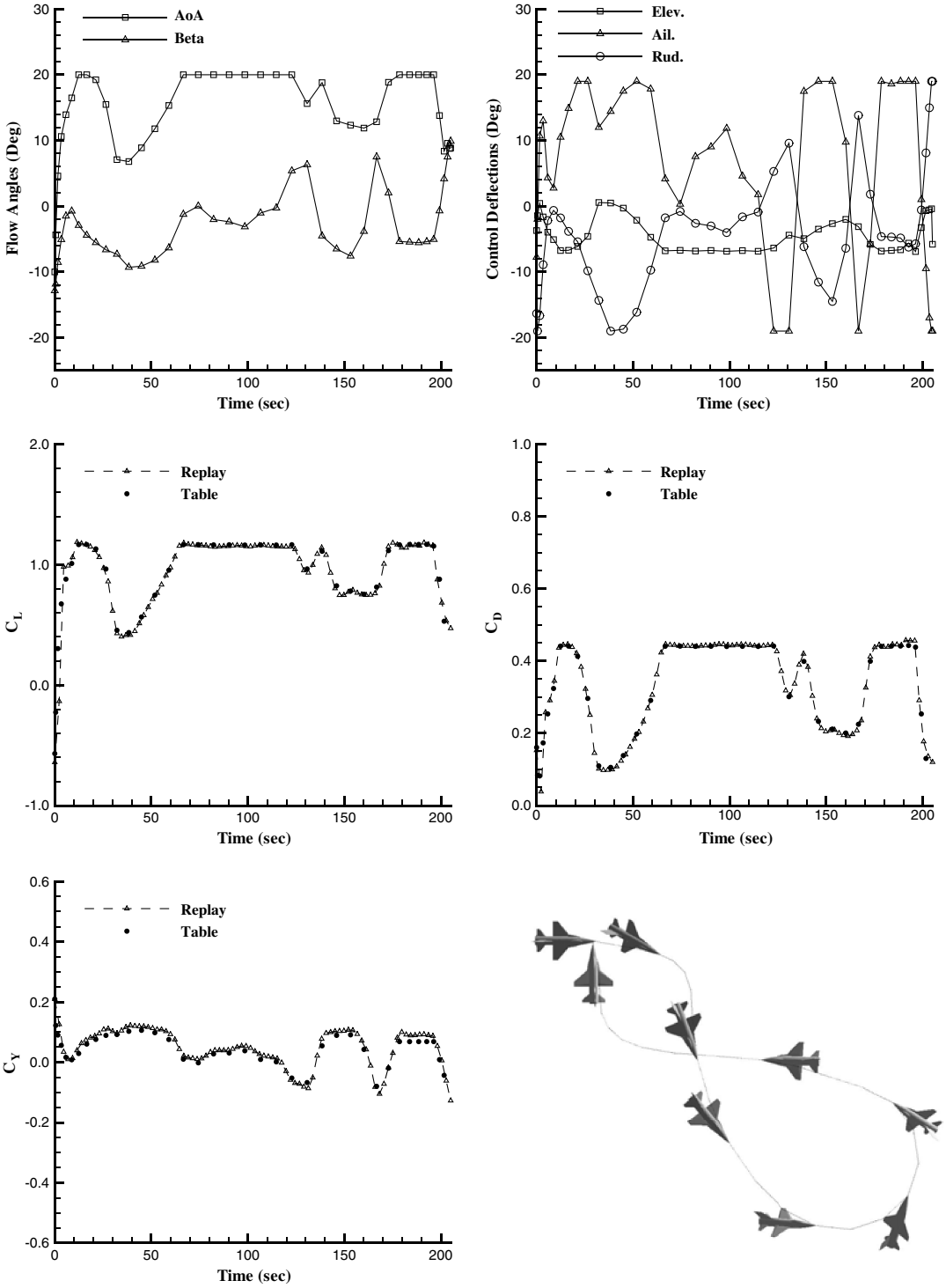

Fig. 11 Turn 90 maneuver definition and replay solution.

106.7 and $V_0 = 121.9$ m/s. The aircraft velocity was then set to achieve the desired relative velocity and angle of attack. The calculation of the lift coefficient for these three cases is shown in Fig. 7 and all three cases give identical values as required.

C. Fixed α Pull-Up Maneuver

Next a pull-up maneuver is considered with the objective to increase the pitch angle by 10 deg. A slow pitch up case with 2 deg/s pitch rate at a fixed value of 9.5° angle of attack is considered. The upper and lower boundary values of the time rates of angle of attack, pitch rate and flight speed are set to $\pm 1.0 \times 10^{-5}$. The elevator deflection angles are limited to ±25°.

The solution is shown in Fig. 8. This shows the trajectory and Hamiltonian. In addition the tabular and replay values for the lift coefficient are shown and are in perfect agreement. Finally the surface pressure contours are shown, with the presence of the weak leading and strake vortices visible.

D. Varying α Pull-Up Maneuver

Removing the constraints imposed to time-rate changes of angle of attack and pitch rate for the fixed α pull-up results in a pull-up with varying angle of attack. To find a slow pull-up, the upper boundary of the pitch rate is again set to 2 deg/s.

The optimum solution results in a pull-up with increasing angle of attack from 0° to nearly 12° in 10 seconds. Dynamic effects are expected to be small at these rates. The elevator varies throughout the motion up to deflections of −2.5°. The maneuver trajectory and time variation of the angle of attack, Mach number and the elevator angle are shown in Fig. 9. The comparison of the tabular and replay values of the lift, drag and pitching moment coefficients are also shown and are in close agreement.

Also shown in Fig. 9 is the replay solution for time steps of 0.125 and 0.5 s, resulting in 80 and 20 time steps for the motion. The results using the two time steps are in close agreement, indicating that the solution obtained using the larger time step is time accurate.

E. Wing-Over

Next, maneuvers featuring lateral motions are considered. A wingover maneuver in 130 s is defined. The predicted time-optimal maneuver changes the heading of the aircraft from 0 to 180°, while the final values of the velocity and altitude are fixed at the initial values. The aircraft gains altitude by increasing its angle of attack, while banking at the same time. At its minimum speed, rudder is applied to change the heading and then the aircraft starts to dive.

The start and final speed and altitude of the minimum time maneuver are set to 91.44 m/s and 914 m, respectively. The optimization is free to choose initial and final angles of attack, but they need to be below 20 deg. Also, throughout time, the angles of attack should not exceed the upper limit of 20 deg. The elevator, aileron, and rudder deflection values are also limited to ±20°. All the rotation angular speeds are limited to small values, resulting in a slow maneuver.

Figure 10 depicts the predicted maneuver. The definition of the angles of attack and side slip are given, together with the control surface deflections. The comparison between the tabular aerodynamics with the replay predictions shows good agreement. This is the case for the two steps used which result in 90 and 180 steps being used to resolve the motion.

F. Turn 90

The final maneuver is a 90 deg turn in 200 s, shown in Fig. 11. The aircraft returns to its original position but with its heading changed by

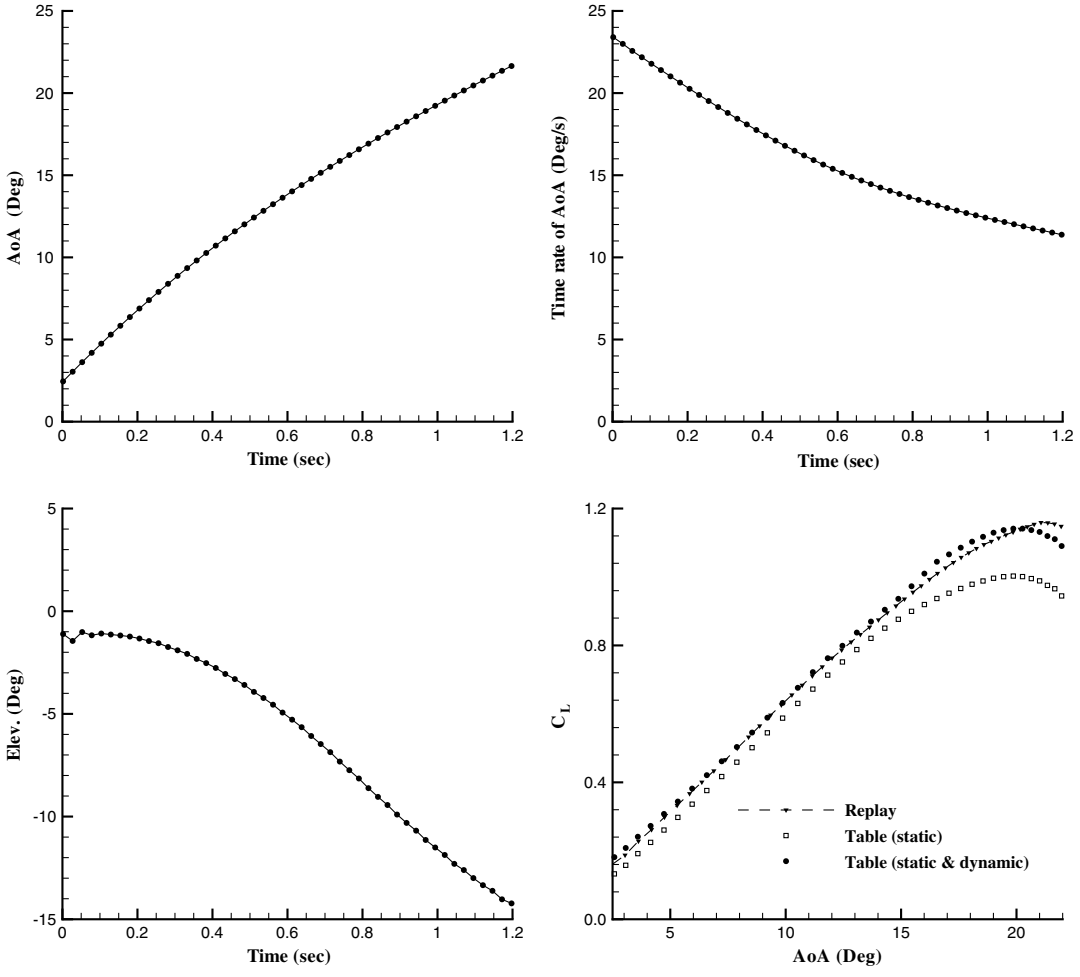

Fig. 12 Medium rate pull-up replay solution.

90 deg. In such a maneuver the final values of the velocity, altitude, latitude, and longitude are fixed to the initial values. Other constraints are similar to those used for the wingover maneuver. The predicted angles of attack and side slip are shown in Fig. 11, together with the control surface deflections. The lift, drag, and side-force coefficients are also shown in Fig. 11 for the replay and the tables are again in close agreement.

VI. Fast Maneuvers

Having demonstrated the agreement between the static tabular and replay predicted aerodynamics for slow motions, we now consider faster maneuvers where we would expect significant dynamic and unsteady effects. Increasingly fast pull-up maneuvers are considered in this section. The dynamic terms which are added to the static tabular values make a significant difference to the forces and moments as the rates are increased. The aim is to evaluate the importance of the dynamic terms, and the presence of unsteady terms that are not represented in the tables.

A medium rate pull-up with time varying angle of attack was defined with an upper limit of 20 deg/s for the pitch rate. The final pitch angle is set such that the aircraft reaches high angles of attack. The optimal solution is shown in Fig. 12. A fast rate maneuver was obtained by increasing the upper boundary value of pitch rate to 100 deg/s. This is shown in Fig. 13. Note that this motion is a purely theoretical example meant to show the ability of the replay to find the

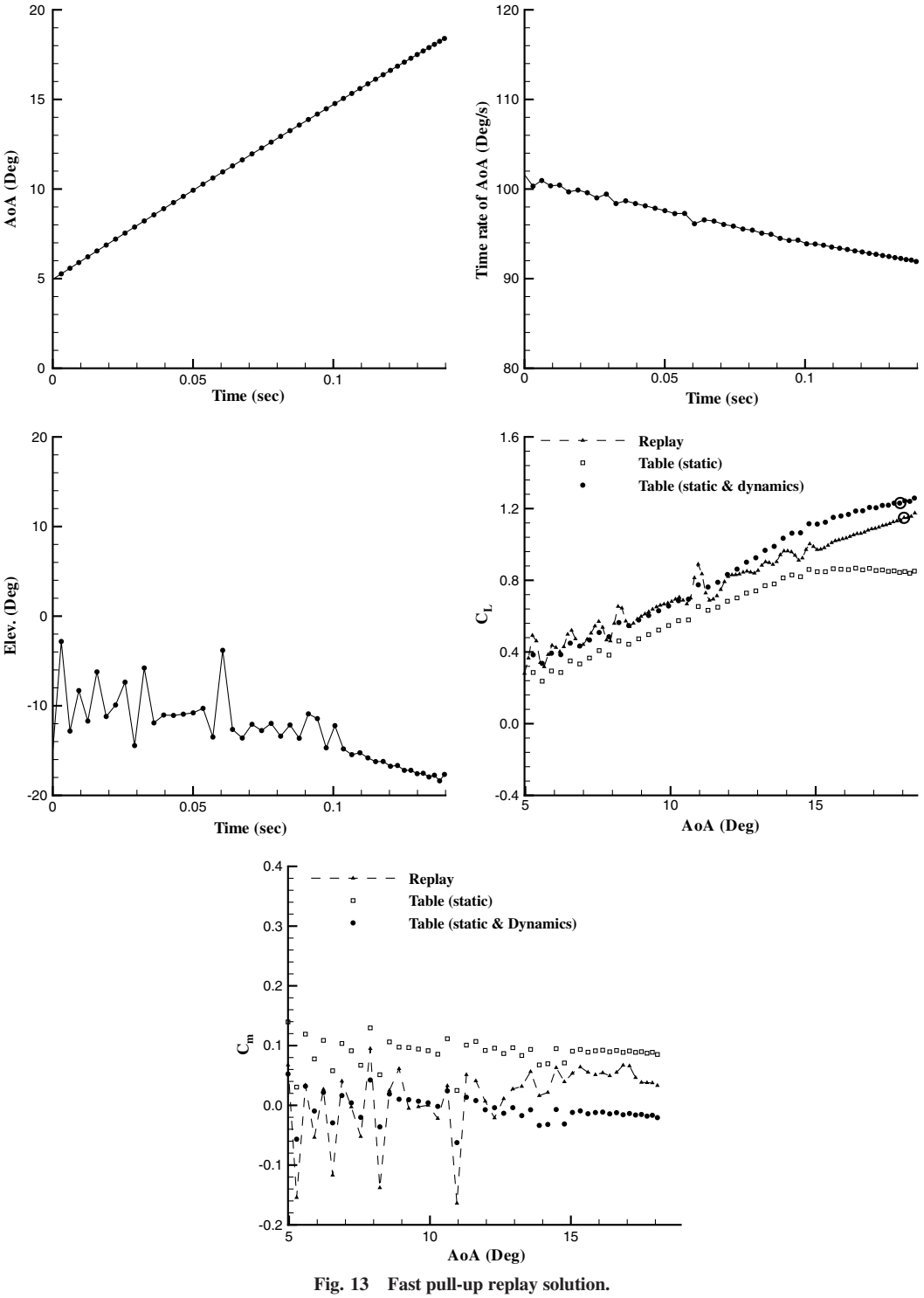

Fig. 13 Fast pull-up replay solution.

limits of validity of the aerodynamic tables, and is not meant to represent a physically achievable motion (which is roughly half the maximum rate for the F-16).

The time variation of the lift coefficients for the medium rate maneuver is shown in Fig. 12. At the low angles the static tabular predictions are close to the replay values, with significant differences at the higher angles when vortical flow is present. The addition of the dynamic tabular terms produces a good agreement with the replay values at the low angles, and a much closer agreement at the higher angles.

The comparison for the fast maneuver is shown in Fig. 13. In this case there is a larger difference between the replay and static tabular predictions at all angles. The addition of dynamic effects makes the tabular predictions close at the lower angles of attack, but cannot correct the discrepancy at the high angles when significant history effects due to vortical interactions are present. Note also the spikes in the lift curve from the replay solution which are due to dynamic effects from the very rapid motion of the control surfaces.

To examine the differences in flow solution when history is present the surface pressure distribution for the fast maneuver is shown in Fig. 14 at one time instant toward the end of the motion, marked with circles in Fig. 13. The time accurate replay result at this instant is compared with a quasi-steady solution which was obtained by calculating the steady-state solution obtained for the aircraft states fixed at the values at the time instant selected. The forces and moments from the quasi-steady solution is in perfect agreement with the tabular value as expected. The motion replay solution shows a weaker leading-edge vortex which leads to a lower value of the lift coefficient. The angle of attack is increasing at this point in the motion and the solution for the replay appears to be lagging the quasi-steady solution.

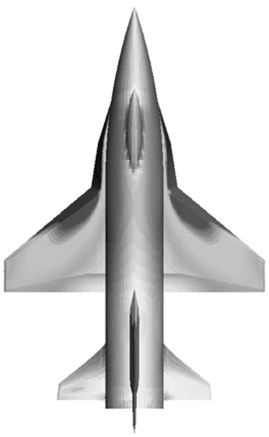

Instantaneous Replay Solution

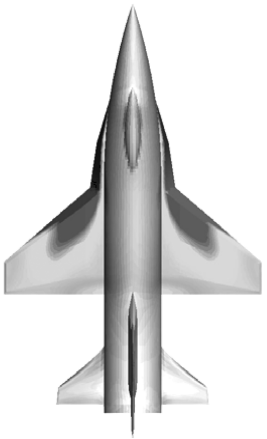

Quasi-steady Solution

Fig. 14 Surface pressure contours for fast maneuver for the points marked with a circle in Fig. 13.

VII. Conclusions

This paper describes a framework for generating optimal maneuvers based on CFD generated tabular aerodynamic models, and then testing the aerodynamic model by replaying the maneuver using an unsteady CFD calculation to check the consistency of the aerodynamic forces and moments. The CFD solver uses two types of mesh movement, namely rigid motion, and transfinite interpolation for the control surfaces. Data fusion was used to allow the generation of the aerodynamic tables in a feasible number of static and forced motion CFD calculations.

The test case used was the SDM generic fighter. Sharp leading edges for the lifting surfaces allowed the Euler equations to be used to demonstrate the framework. A validation was made against available experimental data which showed that the predictions fail to predict static lateral forces and moments above 20 deg when the flowfield is no longer dominated by coherent vortices. The longitudinal dynamic derivatives showed agreement up to 15 deg. To improve the agreement at higher angles viscous modeling is required, with detached eddy simulation a good candidate. However, the agreement at lower angles means that the Euler equations can be used to demonstrate the replay framework, with credible flow physics and predictions being present in the test case.

A number of slow longitudinal and lateral maneuvers were used to demonstrate that the tabular and replay aerodynamics agreed closely as expected. The cost of generating the static tables was the equivalent of 200 steady-state calculations, and the simulation of each maneuver was possible in roughly one tenth of this for the cases shown. Then a number of higher rate maneuvers for a pull-up was used to investigate the influence of dynamic and unsteady terms. At moderate rates the addition of dynamic tabular terms brought the tabular predictions into agreement with the replay values. However, for a high angle of attack, high rate motion, the dynamic terms were not adequate to achieve agreement. A quasi-steady calculation confirmed that the tabular prediction is correct, and so the disagreement is due to the influence of the history in the unsteady replay maneuver. This example shows the usefulness of the framework in investigating the limits of the tabular aerodynamic models.

Future work will extend this study to include URANS and DES flow modeling to capture high angle of attack vortical flows more realistically than can be achieved with the Euler modeling used in this study. The discrepancy between the time step needed by DES to resolve the turbulence and the relatively long time scales of the motion make this a challenging computational task. The framework is being applied to a fighter trainer aircraft with flight test data available to compare with. Finally, the impact of vortical flow history effects will be investigated, and previous work on modeling these effects reconsidered. Note that the framework can be extended to consider other forms of aerodynamic model, such as state space models.

Acknowledgments

This work was supported by the Engineering and Physical Sciences Research Council and the Ministry of Defence under EP/D504473/1. Da Ronch was supported by the SimSAC project under funding from the Sixth Framework programme of the European Union, Swift by a BAE SYSTEMS/ Engineering and Physical Sciences Research Council studentship, and Marques by the European Union under the Marie Curie Excellence Team ECERTA, contract MEXT-CT-2006 042383. Computer time was provided though the UK Applied Aerodynamics Consortium under EPSRC grant EP/F005954/1.

References

[1] Hamel, P. G., and Jategaonkar, R. V., "Evolution of Flight Vehicle System Identification," *Journal of Aircraft*, Vol. 33, No. 1, 1996, pp. 9–28.
doi:10.2514/3.46898

[2] Jouannet, C., and Krus, P., "Lift Coefficient Predictions for Delta Wing Under Pitching Motions," *32nd AIAA Fluid Dynamics Conference and Exhibit*, AIAA Paper 2002-2969, June 2002.

[3] Katz, J., and Schiff, L. B., "Modeling Aerodynamic Responses to Aircraft Maneuvers: A Numerical Validation," *Journal of Aircraft*, Vol. 23, No. 1, 1986, pp. 19–25. doi:10.2514/3.45261

[4] Greenwell, D. I., "A Review of Unsteady Aerodynamic Modelling for Flight Dynamics of Manoeuvrable Aircraft," *AIAA Atmospheric Flight Mechanics Conference and Exhibit*, AIAA Paper 2004-5276, Aug. 2004.

[5] Park, M., Green, L., Montgomery, R., and Raney, D., "Determination of Stability and Control Derivatives Using Computational Fluid Dynamics and Automatic Differentiation," *17th AIAA Applied Aerodynamics Conference*, AIAA Paper 99-3136, June 1999.

[6] Simon, J. M., "Dynamic Derivative Data for High-Angle-of-Attack Simulation," *10th Applied Aerodynamics Conference*, AIAA Paper 92-4355, Aug. 1992.

[7] Park, M. A., and Green, L. L., "Steady-State Computation of Constant Rotational Rate Dynamic Stability Derivatives," *18th AIAA Applied Aerodynamics Conference*, AIAA Paper 2000-4321, Aug. 2000.

[8] Kay, Jacob, "Acquiring and Modeling Unsteady Aerodynaimc Characteristics," *AIAA Atmospheric Flight Mechanics Conference and Exhibit*, AIAA Paper 2000-3907, Aug. 2000.

[9] Murman, S. M., Pandya, S. A., and Chaderjian, N. M., "Automation of a Navier–Stokes S and C Database Generation for the Harrier in Ground Effect," *40th AIAA Aerospace Sciences Meeting and Exhibit*, AIAA Paper 2002-259, Jan. 2002.

[10] Ghoreyshi, M., Badcock, K. J., and Woodgate, M., "Accelerating the Numerical Generation of Aerodynamic Models for Flight Simulation," *Journal of Aircraft*, Vol. 46, No. 3, 2009, pp. 972–980. doi:10.2514/1.39626

[11] Harper, P. W., and Flanigan, R. E., "The Effect of Change of Angle of Attack on the Maximum Lift of a Small Model," National Advisory Committee for Aeronautics, NACA TN-2061, March 1950.

[12] Levy, L. L., and Tobak, M., "Nonlinear Aerodynamics of Bodies of Revolution in Free Flight," *AIAA Journal*, Vol. 8, No 12, 1970, pp. 2168–2171. doi:10.2514/3.6082

[13] Tobak, M., and Schiff, L. B., "Generalized Formulation of Nonlinear Pitch-Yaw-Roll Coupling. Part 1: Nonaxisymmetric Bodies," *AIAA Journal*, Vol. 13, No. 3, 1975, pp. 323–326. doi:10.2514/3.49698

[14] Tobak, M., and Schiff, L. B., "Generalized Formulation of Nonlinear Pitch-Yaw-Roll Coupling. Part 2: Nonlinear Coning-Rate Dependence," *AIAA Journal*, Vol. 13, No. 3, 1975, pp. 327–332. doi:10.2514/3.49699

[15] Abramov, N. B., Goman, M. G., Greenwell, D. I., and Khrabrov, A. N., "Two-Step Linear Regression Methods for Identification of High Incidence Unsteady Aerodynamic Model," *AIAA Atmospheric Flight Mechanics Conference and Exhibit*, AIAA Paper 2001-4080, Aug., 2001.

[16] Ballhaus, W. F., and Goorjian, P. M., "Computation of Unsteady Transonic Flow by the Indicial Method," *AIAA Journal*, Vol. 16, No. 2, 1978, pp. 117–124. doi:10.2514/3.60868

[17] Rizzetta, D. P., "Time-Dependent Response of a Two-Dimensional Airfoil in Transonic Flow," *AIAA Journal*, Vol. 17, No. 1, 1979, pp. 26–32. doi:10.2514/3.61058

[18] Chyu, W. J., and Schiff, L. B., "Nonlinear Aerodynamic Modeling of Flap Oscillations in Transonic Flow: A Numerical Validation," *AIAA Journal*, Vol. 21, No. 1, 1983, pp. 106–113. doi:10.2514/3.8035

[19] Steger, J. L., and Bailey, H. E., "Calculation of Transonic Aileron Buzz," *AIAA Journal*, Vol. 18, No. 3, 1980, pp. 249–255. doi:10.2514/3.50756

[20] Schutte, A., Einarsson, G., Raichle, A., Schoning, B., Mönnich, W., and Forkert, T., "Numerical Simulation of Manoeuvreing Aircraft by Aerodynamic, Flight Mechanics, and Structural Mechanics Coupling," *Journal of Aircraft*, Vol. 46, No. 1, 2009, pp. 53–64. doi:10.2514/1.31182

[21] Badcock, K. J., Richards, B. E., and Woodgate, M. A., "Elements of Computational Fluid Dynamics on Block Structured Grids Using Implicit Solvers," *Progress in Aerospace Sciences*, Vol. 36, Nos. 5–6, 2000, pp. 351–392. doi:10.1016/S0376-0421(00)00005-1

[22] Osher, S., and Chakravarthy, S., "Upwind Schemes and Boundary Conditions with Applications to Euler Equations in General Geometries," *Journal of Computational Physics*, Vol. 50, No. 3, 1983, pp. 447–481. doi:10.1016/0021-9991(83)90106-7

[23] Van Leer, B., "Towards the Ultimate Conservative Conservative Difference Scheme 2: Monotonicity and Conservation Combined in a Second Order Scheme," *Journal of Computational Physics*, Vol. 14, No. 4, 1974, pp. 361–374. doi:10.1016/0021-9991(74)90019-9

[24] Boelens, O. J., Badcock, K. J., Elmilgui, A., Abdol-Hamid, K. S., and Massey, S. J., "Comparison of Measured and Block Structured Simulation Results for the F-16XL Aircraft," *Journal of Aircraft*, Vol. 46, No. 2, 2009, pp. 377–384. doi:10.2514/1.35064

[25] Rampurawala, A. M., and Badcock, K. J., "Evaluation of a Simplified Grid Treatment for Oscillating Trailing-Edge Control Surfaces," *Journal of Aircraft*, Vol. 44, No. 4, 2007, pp. 1177–1188. doi:10.2514/1.24623

[26] Allan, M. R., Badcock, K. J., and Richards, B. E., "CFD Based Simulation of Longitudinal Flight Mechanics with Control," *43rd AIAA Aerospace Science Meeting and Exhibition*, AIAA Paper 2005-46, 2005.

[27] Beyers, M. E., "Subsonic Roll Oscillation Experiments on the Standard Dynamics Model," *AIAA Atmospheric Flight Mechanics Conference*, AIAA Paper 83-2134, 1983.

[28] Jermey, C., and Schiff, L. B., "Wind Tunnel Investigation of the Aerodynamic Characterestics of the Standard Dynamic Model in Coning Motion at Mach 0.6," *12th Atmospheric Flight Mechanics Conference*, AIAA Paper 85-1828, 1985.

[29] Alemdaroglu, N., Iyigun, I., Altun, M., Uysal, H., Quagliotti, F., and Guglieri, G., "Determination of Dynamic Stability Derivatives Using Forced Oscillation Technique," *40th Aerospace Sciences Meeting and Exhibition*, AIAA Paper 2002-0528, 2002.

[30] Davari, A. R., and Soltani, M. R., "Effects of Plunging Motion on Unsteady Aerodynamic Behaviour of an Aircraft Model in Compressible Flow," *Iranian Journal of Science and Technology, Transaction B: Engineering*, Vol. 31, No. B1, 2007, pp. 49–63.

[31] Winchenback, G. L.,, Uselton, R. L., Hathaway, W. H., and Chelekis, R. M., "Free-Flight and Wind-Tunnel Data for a Generic Fighter Configuration," *Journal of Aircraft*, Vol. 21, No. 1, 1984, pp. 361–381.

[32] Williams, J. E., and Vukelich, S. R., "The USAF Stability and Control Digital DATCOM," *McDonnell Douglas Astona UTICS Company*, AFFDL TR-79-3032, St. Louis, MO, 1979.

[33] Huang, X. Z., "Wing and Fin Buffet on the Standard Dynamic Model," NATO RTO Rept. Number RTO-TR-26, pp. 361–381; also Winchenback, G. L., Uselton, R. L., Hathaway, W. H., and Chelekis, R. M., "Free-Flight and Wind-Tunnel Data for a Generic Fighter Configuration," *Journal of Aircraft*, Vol. 21, No. 1, 1984, pp. 5–13.

[34] Cook, M., and V., *Flight Dynamics Principles*, John Wiley, New York, 2007.

[35] Brinkman, K., and Visser, H. G., "Optimal Turn-Back Maneuver After Engine Failure in a Single-Engine Aircraft During Climb-Out," *Journal of Aerospace Engineering, Part G*, Vol. 221, No. 1, 2006, pp. 17–27. doi:10.1243/09544100JAERO116

[36] Steven, B. L., and Lewis, F. L., *Aircraft Control and Simulation*, Wiley, New York, 1992.

[37] Ross, I., Sekhavat, P., Fleming, A., Gong, Q., and Wei Kang, W., "Pseudospectral Feedback Control: Foundations, Examples and Experimental Results," *AIAA Guidance, Navigation, and Control Conference and Exhibit*, AIAA Paper 2006-6354, Aug. 2006.